

Research Paper

Synechococcus elongatus PCC7942 secretes extracellular vesicles to accelerate cutaneous wound healing by promoting angiogenesis

Hao Yin^{1,2*}, Chun-Yuan Chen^{1,2*}, Yi-Wei Liu^{2,3*}, Yi-Juan Tan², Zhi-Li Deng^{4,8}, Fei Yang⁷, Fei-Yu Huang⁷, Cong Wen⁷, Shan-Shan Rao^{2,9}, Ming-Jie Luo^{2,9}, Xiong-Ke Hu², Zheng-Zhao Liu^{2,3,4,6}, Zhen-Xing Wang², Jia Cao², Hao-Ming Liu², Jiang-Hua Liu^{1,2}, Tao Yue^{1,2}, Si-Yuan Tang⁹, Hui Xie^{1,2,3,4,5,6}✉

1. Department of Orthopedics, Xiangya Hospital, Central South University, Changsha, Hunan 410008, China.
2. Movement System Injury and Repair Research Center, Xiangya Hospital, Central South University, Changsha, Hunan 410008, China.
3. Department of Sports Medicine, Xiangya Hospital, Central South University, Changsha, Hunan 410008, China.
4. Hunan Key Laboratory of Organ Injury, Aging and Regenerative Medicine, Changsha, Hunan 410008, China.
5. Hunan Key Laboratory of Bone Joint Degeneration and Injury, Changsha, Hunan 410008, China.
6. National Clinical Research Center for Geriatric Disorders, Xiangya Hospital, Central South University, Changsha, Hunan 410008, China.
7. Department of Occupational and Environmental Health, Xiangya School of Public Health, Central South University, Changsha, Hunan 410078, China.
8. Department of Dermatology, Xiangya Hospital, Central South University, Changsha, Hunan 410008, China.
9. Xiangya Nursing School, Central South University, Changsha, Hunan 410013, China

*These authors contributed equally to this work.

✉ Corresponding author: huixie@csu.edu.cn; #87 Xiangya road, Changsha, Hunan 410008, China.

© Ivyspring International Publisher. This is an open access article distributed under the terms of the Creative Commons Attribution (CC BY-NC) license (<https://creativecommons.org/licenses/by-nc/4.0/>). See <http://ivyspring.com/terms> for full terms and conditions.

Received: 2018.11.29; Accepted: 2019.02.17; Published: 2019.04.13

Abstract

Poor wound healing affects millions of people worldwide each year and needs better therapeutic strategies. *Synechococcus elongatus* PCC 7942 is a naturally occurring photoautotrophic cyanobacterium that can be easily obtained and large-scale expanded. Here, we investigated the therapeutic efficacy of this cyanobacterium in a mouse model of acute burn injury and whether the secretion of extracellular vesicles (EVs), important mediators of cell paracrine activity, is a key mechanism of the cyanobacterium-induced regulation of wound healing.

Methods: The effects of *Synechococcus elongatus* PCC 7942 on burn wound healing in mice under light or dark conditions were evaluated by measuring wound closure rates, histological and immunofluorescence analyses. A series of assays *in vivo* and *in vitro* were conducted to assess the impact of the cyanobacterium on angiogenesis. GW4869 was used to interfere with the secretion of EVs by the cyanobacterium and the abilities of the GW4869-pretreated and untreated *Synechococcus elongatus* PCC 7942 to regulate endothelial angiogenesis were compared. The direct effects of the cyanobacterium-derived EVs (*S. elongatus*-EVs) on angiogenesis, wound healing and expressions of a class of pro-inflammatory factors that have regulatory roles in wound healing were also examined.

Results: *Synechococcus elongatus* PCC 7942 treatment under light and dark conditions both significantly promoted angiogenesis and burn wound repair in mice. *In vitro*, the cyanobacterium enhanced angiogenic activities of endothelial cells, but the effects were markedly blocked by GW4869 pretreatment. *S. elongatus*-EVs were capable of augmenting endothelial angiogenesis *in vitro*, and stimulating new blood vessel formation and burn wound healing in mice. The expression of interleukin 6 (IL-6), which has an essential role in angiogenesis during skin wound repair, was induced in wound tissues and wound healing-related cells by *S. elongatus*-EVs and *Synechococcus elongatus* PCC 7942.

Conclusion: *Synechococcus elongatus* PCC 7942 has the potential as a promising strategy for therapeutic angiogenesis and wound healing primarily by the delivery of functional EVs, not by its photosynthetic activity. The promotion of IL-6 expression may be a mechanism of the cyanobacterium and its EVs-induced pro-angiogenic and -wound healing effects.

Key words: *Synechococcus elongatus* PCC 7942, extracellular vesicles, wound healing, angiogenesis

Introduction

The skin is the largest organ in the human body and acts as a functional barrier against water loss, pathogen invasion and ultraviolet radiation. However, the integrity of the skin is frequently damaged by acute and chronic injuries such as extensive burn and diabetic ulceration, causing physical and mental suffering as well as financial burden to the patients and their families [1]. Hence, numerous ongoing investigations are focusing on accelerating the wound healing process. Angiogenesis is essential to replace damaged capillaries and deliver oxygen and nutrients to wounded tissue, thus promoting the proliferation and migration of fibroblasts and keratinocytes, collagen synthesis and re-epithelialization, all of which are processes vital for skin wound healing [2, 3]. Thus, therapeutic angiogenesis has emerged as a promising strategy for the acceleration of healing of acute and chronic wounds [3, 4].

The cyanobacterium *Synechococcus elongatus* (*S. elongatus*) PCC 7942 is a unicellular, obligate photoautotroph that represents a preeminent model for studying photosynthesis and circadian rhythms [5, 6]. This model strain is being developed for the bioproduction of fuels, industrial chemicals and pharmaceuticals [5, 7-9]. It is attractive for this purpose due to its genetic tractability and its ability to utilize light, carbon dioxide, and water as energy for metabolism, thus reducing the environmental and economic costs of cultivation [10]. Recently, by using light as a source of energy, Cohen et al demonstrated that intramyocardial delivery of *S. elongatus* PCC 7942 to the rat ischemic heart greatly increases tissue oxygenation, maintains myocardial metabolism and augments cardiac function [11]. Moreover, this novel therapeutic system seems to be nontoxic and does not elicit an obvious immune response [11], suggesting a promising prospect for future use of *S. elongatus* PCC 7942 to treat ischemic diseases. This study prompted us to explore whether local transplantation of *S. elongatus* PCC 7942 can speed up the wound healing process via enhancing tissue oxygenation through photosynthesis. However, in the present study, we unexpectedly found that transplantation of these cyanobacteria significantly promoted angiogenesis and wound repair in a mouse model of acute burn injury under both light and dark conditions, suggesting that there must exist other important mechanism that mediates the therapeutic effects of *S. elongatus* PCC 7942.

Secretion of extracellular vesicles (EVs) is a common feature of both eukaryotic and prokaryotic cells [12]. EVs are now considered as key mediators of

cell paracrine activity by transferring parent cells-derived functional proteins, lipids and nucleic acids into target cells to regulate their biological activity [12-14]. Accumulating studies have shown that stem cells-derived EVs can be exploited directly as potential therapeutic agents for tissue regeneration. EVs, with fewer safety considerations relative to their parent cells after transplantation, provide a novel strategy to stimulate wound repair and regeneration [15, 16]. In a recent study, we have shown that EVs from human urine-derived stem cells have the ability to augment the function of skin cells and accelerate diabetic wound healing in mice [17]. In heterotrophic Gram-negative bacteria, 20-250 nm sized EVs, also called outer membrane vesicles (OMVs), can be formed when regions of the outer membrane “pinch off” from the cells and the roles of these EVs have been extensively characterized [18-20]. Recently, Biller et al reported for the first time that the photoautotrophic cyanobacterium *Prochlorococcus* can continuously release EVs that are able to support the growth of heterotrophic bacterial cultures [18]. Thereafter, Pardo et al identified that the cyanobacterium *Synechocystis* PCC 6803 naturally produces outer membrane-derived EVs [21]. To date, however, EVs production has not been described in *S. elongatus* PCC 7942. Considering the key role of EVs in cell activity [12], we were interested to know whether the secretion of EVs is a critical mechanism that mediates the pro-angiogenic and -wound healing effects of *S. elongatus* PCC 7942.

In the work described here, after determining the beneficial effects of *S. elongatus* PCC 7942 on angiogenesis and wound healing in a mouse full-thickness burn model, we then tested the impact of the cyanobacteria on angiogenic activities of cultured endothelial cells and determined the contribution of EVs in this process. Further, we investigated whether direct treatment with *S. elongatus* PCC 7942-derived EVs (*S. elongatus*-EVs) is sufficient to promote angiogenesis and accelerate the repair process of burn wounds. This study aimed to explore an entirely novel application for *S. elongatus* PCC 7942 in regenerative medicine and uncover a new mechanism by which *S. elongatus* PCC 7942 exerts function.

Results

***S. elongatus* PCC 7942 accelerates the healing of cutaneous burn wounds**

To investigate whether *S. elongatus* PCC 7942 can provide therapeutic benefits to cutaneous wounds, two full-thickness burn wounds were created on the back of each mice, followed by subcutaneous injection

of *S. elongatus* PCC 7942 (10^5 cells in 100 μ L PBS) in the light (*S. elongatus*-light) or in the dark (*S. elongatus*-dark), or injection of an equal volume of vehicle control (PBS). The mice in the *S. elongatus*-light and control groups were kept under standard laboratory condition (12 h light/dark cycles) after injection. In the *S. elongatus*-dark group, injections were performed under dimmed room light and the mice were kept under dark condition for 24 h after injection. Digital photographs of wounds showed that both the mice treated with *S. elongatus* PCC 7942 in the light and dark exhibited much faster wound closure compared to the PBS-treated mice, as determined by smaller wound areas measured at day 3, 7 and 12 post-wounding (**Figure 1A-B**). The rate of wound closure in the *S. elongatus*-light group was slightly higher than that in *S. elongatus*-dark group, but only by trend (**Figure 1A-B**). As evidenced by H&E staining, the wounds receiving *S. elongatus* PCC 7942 injections both in the light and in the dark showed much longer newly formed epidermis and dermis with regenerated hair follicles and fat cells compared to the PBS-treated control wounds at day 12 after operation (**Figure 1C**). Quantification of the rate of re-epithelialization and scar widths revealed that *S. elongatus* PCC 7942 under both light and dark conditions was capable of enhancing re-epithelialization and reducing scar formation (**Figure 1D**). Masson's trichrome staining showed that collagen deposition in the *S. elongatus*-light and -dark groups were slightly increased relative to the control group, but the differences were not statistically significant (**Figure 1E-F**), suggesting that *S. elongatus* PCC 7942 does not cause excessive collagen accumulation. Ki67 immunostaining was performed to test the proliferation of skin cells in the wound sites. As shown in **Figure 1G** and **H**, a greater numbers of ki67-positive proliferating skin cells appeared in the wounds transplanted with *S. elongatus* PCC 7942 both in the light and dark, as compared with the wounds treated with PBS. No significant differences were observed in the numbers of proliferating skin cells between *S. elongatus*-light and -dark groups (**Figure 1G-H**). These results indicate that *S. elongatus* PCC 7942 is able to promote the healing of burn wounds regardless of whether it is in the light or dark, suggesting that the beneficial effects of *S. elongatus* PCC 7942 on wound healing is not primarily mediated by enhancing tissue oxygenation through photosynthesis.

In the process of wound healing, keratinocytes' migration and proliferation are the crucial steps during re-epithelialization and fibroblasts are mainly responsible for collagen synthesis and wound contraction [22, 23]. To test whether the promotion of

function of keratinocytes and fibroblasts contributes to the pro-wound healing effects of *S. elongatus* PCC 7942, we assessed its impact on the proliferation and migration of human skin keratinocyte cell line HaCaT and human skin fibroblasts (HSFs) *in vitro*. As the *in vivo* data showed that *S. elongatus* PCC 7942 either in the light or dark could both induce significant beneficial effects, the cyanobacteria (10^6 cells/mL) were incubated under standard condition with the recipient cells without being given the extra light, once they were added to the culture medium of the recipient cells. Cell counting kit-8 (CCK-8) analysis was applied to measure the proliferation of cells. Unexpectedly, the results revealed that incubation with *S. elongatus* PCC 7942 profoundly suppressed the proliferation of HaCaT and HSFs (**Figure S1A**). The scratch wound healing assay showed that co-culture with *S. elongatus* PCC 7942 enhanced the motility of HaCaT (**Figure S1B-C**), but the migration of HSFs was inhibited after exposure to *S. elongatus* PCC 7942, as evidenced by the transwell migration assay (**Figure S1D-E**). Most of these results were not in accordance with the above-described *in vivo* data showing that *S. elongatus* PCC 7942 transplantation facilitated wound closure, epidermal regeneration, skin cell proliferation and normal collagen deposition in the burn wounds, suggesting that the pro-wound healing effects of *S. elongatus* PCC 7942 are not exerted primarily through direct stimulation of keratinocytes and fibroblasts.

***S. elongatus* PCC 7942 enhances angiogenesis in the wound sites**

In consideration of the critical role of angiogenesis in wound healing, we next asked whether *S. elongatus* PCC 7942 transplantation influences the angiogenic activities in the wound sites. Skin images from the undersurface showed that the wounds receiving *S. elongatus* PCC 7942 treatment under light or dark conditions both exhibited much more newly formed blood vessels compared to the PBS-treated control wounds at day 12 post-wounding (**Figure 2A**). Dermal microvessels were then immunostained for the endothelial marker CD31. As shown in **Figure 2B**, a larger numbers of blood vessels were observed in the wounds treated with *S. elongatus* PCC 7942 both in the light and dark when compared to the control wounds. Quantitative measurement of the numbers of CD31-positive vessel structures confirmed that *S. elongatus* PCC 7942 was capable of enhancing angiogenesis in the wound areas either in the light or in the darkness (**Figure 2C**). These data suggest that the pro-angiogenic effects of *S. elongatus* PCC 7942 are not directly relevant to its photosynthetic activity and the promotion of angiogenesis may be an important factor that

contributes to *S. elongatus* PCC 7942- induced acceleration of wound healing.

Angiogenesis is defined as the formation of new blood vessels from pre-existing vasculature by proliferation, migration and tube formation of vascular endothelial cells [2]. Thus, we evaluated the effects of *S. elongatus* PCC 7942 (10^6 cells/mL) on the angiogenic activities of endothelial cells *in vitro*. CCK-8 assay showed that human microvascular endothelial cells (HMECs) treated with *S. elongatus* PCC 7942 showed a significant higher proliferative ability compared to the PBS-treated HMECs (Figure 2D). Transwell assay (Figure 2E-F) and scratch wound healing assay (Figure 2G-H) revealed that

incubation with *S. elongatus* PCC 7942 remarkably increased the migration of HMECs. Tube formation assay showed that when compared with the control HMECs, a higher number of capillary-like structures were formed in HMECs treated with *S. elongatus* PCC 7942 (Figure 2I). The total tube length, total branching points and total loops were measured to quantify the ability of HMECs to form tubes. As shown in Figure 2J, all these indicators were markedly increased once the cells were exposed to *S. elongatus* PCC 7942. These findings indicate that *S. elongatus* PCC 7942 has the ability to augment the angiogenic activities of endothelial cells.

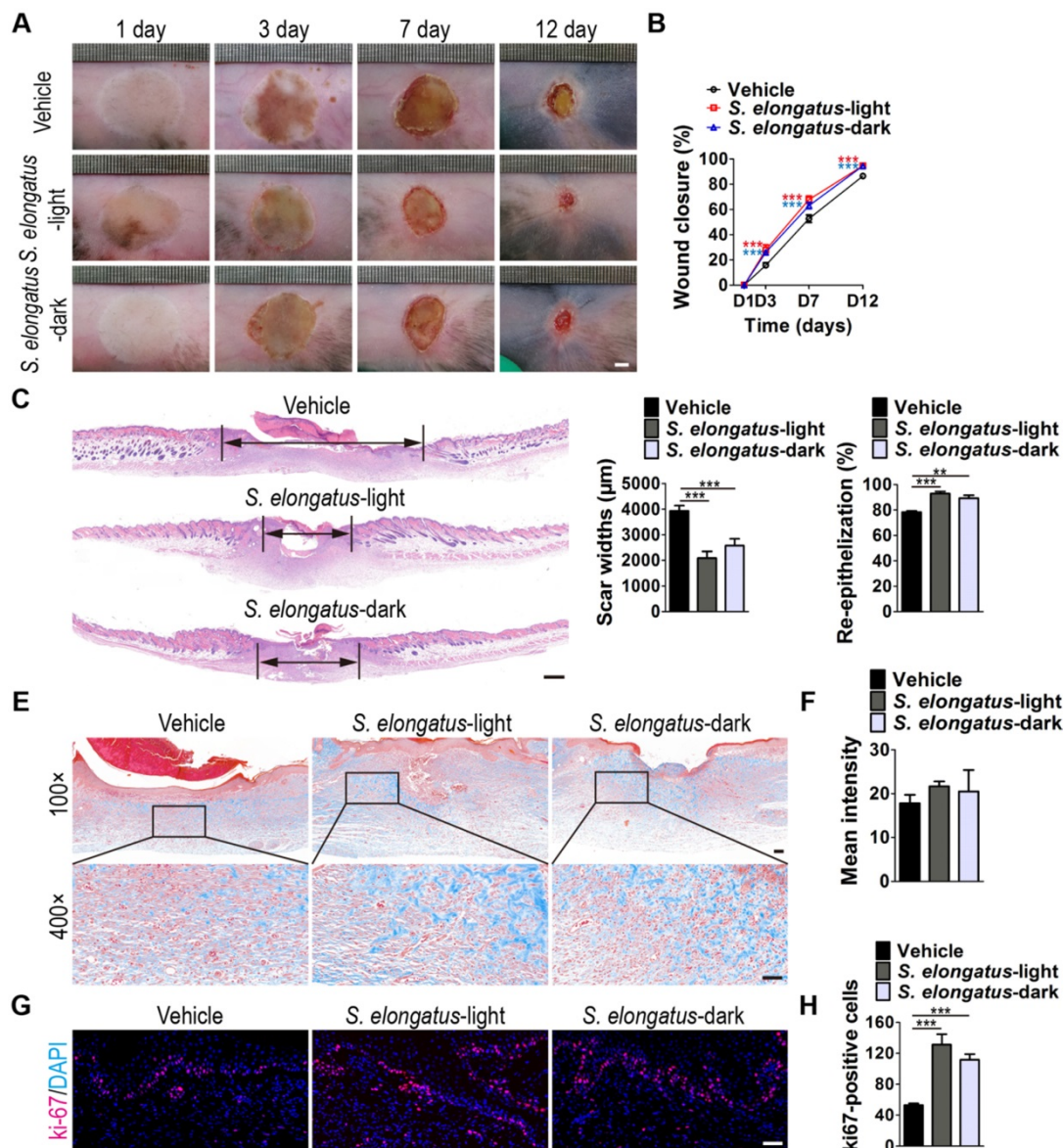


Figure 1. *S. elongatus* PCC 7942 accelerates the healing of cutaneous burn wounds. (A) Representative images of wounds treated with PBS, *S. elongatus* PCC 7942 in the light (*S. elongatus*-light) and *S. elongatus* PCC 7942 in the dark (*S. elongatus*-dark) at days 3, 7 and 12 post-wounding. Scale bar: 2 mm. (B) The rate of wound closure at the indicated times. n = 10 per group. (C) Representative H&E staining images of wound sections at day 12 post-wounding. The black double-headed arrows indicate the edges of scars. Ep: epithelium. Scale bar: 500 µm. (D) Quantification of the rate of re-epithelialization and scar widths. n = 3 per group. (E) Representative images of Masson's trichrome stained-wound sections at day 12 post-wounding. Scale bar: 100 µm (top) or 50 µm (bottom). (F) Quantification of the mean intensity of Masson-stained areas. n = 3 per group. (G) Representative images of ki67-stained wound sections at day 12 post-wounding. Scale bar: 50 µm. (H) Quantification of the number of ki67-positive cells. n = 3 per group. Data are plotted as mean ± SD. *P < 0.05, **P < 0.01, ***P < 0.001.

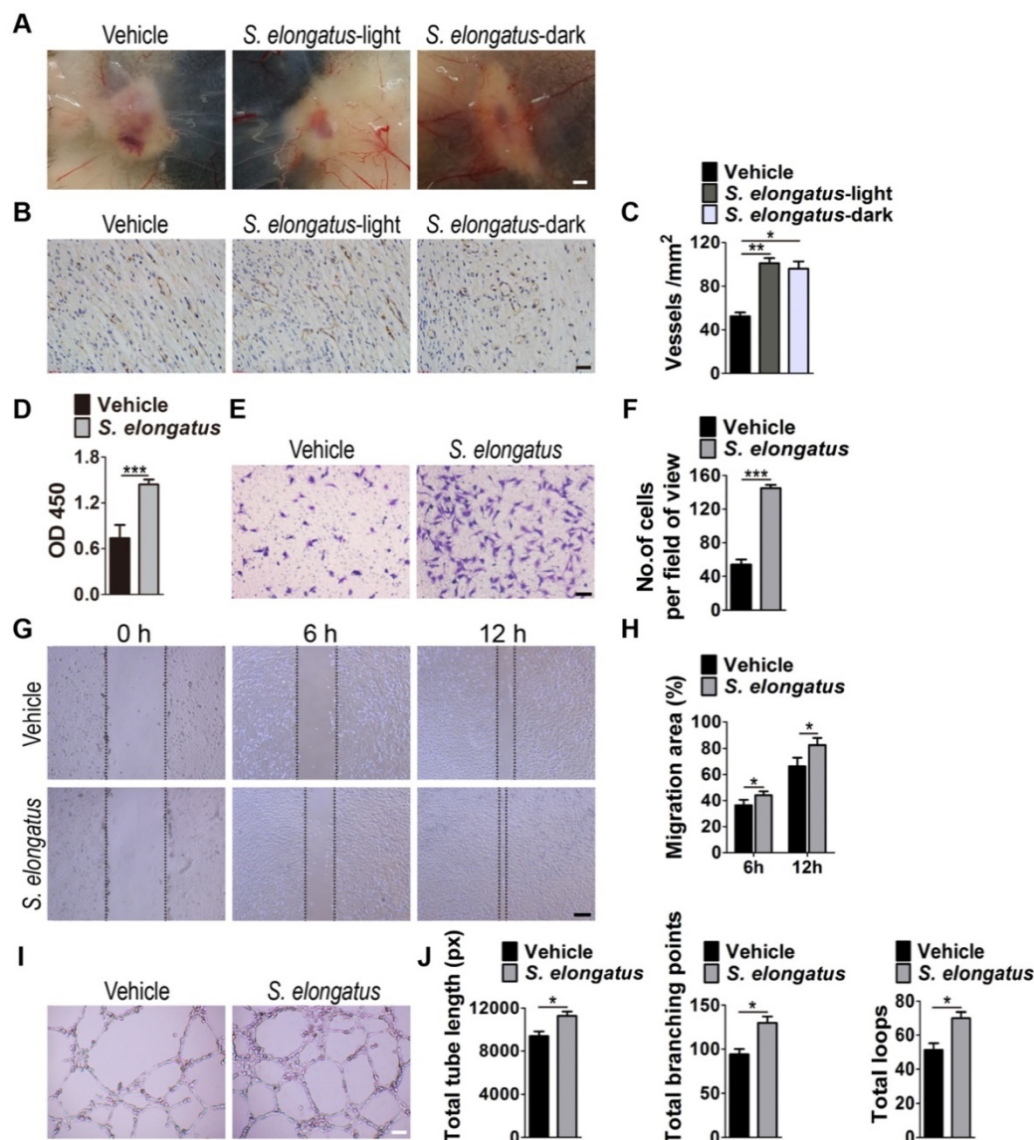


Figure 2. *S. elongatus* PCC 7942 enhances angiogenesis *in vivo* and *in vitro*. (A) Gross view of wounds treated with PBS, *S. elongatus*-light and *S. elongatus*-dark at day 12 post-wounding from the undersurface. Scale bar: 2 mm. (B) Representative images of vascular marker CD31-stained wound sections at day 12 post-wounding. Scale bar: 50 μ m. (C) Quantification of the number of CD31-positive vessels. n = 3 per group. (D) CCK-8 analysis of proliferation of human microvascular endothelial cells (HMECs). n = 4 per group. (E-F) Representative images of transwell migration assay in HMECs (E) and quantification of the migrated cells (F). Scale bar: 100 μ m. n = 3 per group. (G-H) Representative images of wound healing assay in HMECs (G) and quantification of the migration rates (H). Scale bar: 200 μ m. n = 3 per group. (I) Representative images of HMECs' tube formation. Scale bar: 200 μ m. (J) Quantification of the total tube length, total branching points and total loops. n = 3 per group. Data are plotted as mean \pm SD. * P < 0.05, ** P < 0.01, *** P < 0.001.

EVs mediate the pro-angiogenic effects of *S. elongatus* PCC 7942

Next, we examined whether EVs are involved in *S. elongatus* PCC 7942-induced promotion of angiogenesis of endothelial cells by using GW4869, a specific inhibitor of neutral sphingomyelinase-2 that is capable of impairing release of EVs [24]. As shown in Figure 3A, EVs secretion was profoundly suppressed once *S. elongatus* PCC 7942 was treated with GW4869, as indicated by the significant decrease of total protein contents of isolated EVs. Even though GW4869 was removed from the culture medium for 24 h, the secretion of EVs was still much lower than that in the control groups (Figure 3A). We added the

GW4869-pretreated *S. elongatus* PCC 7942 to cultures of HMECs and found that the ability of the cyanobacteria to promote the proliferation, migration and tube formation of HMECs was markedly abolished by GW4869 pre-treatment, as evidenced by CCK-8 analysis (Figure 3B), transwell migration assay (Figure 3C-D), scratch wound healing assay (Figure 3E-F) and tube formation assay on Matrigel (Figure 3G-H), respectively.

Subsequently, we assessed the direct effects of *S. elongatus* PCC 7942-derived EVs (*S. elongatus*-EVs) on endothelial angiogenesis. By using transmission electron microscopy and dynamic light scattering analysis, we first detected the production of EVs by *S.*

elongatus PCC 7942. As shown in **Figure 4A-B**, these vesicles exhibited a spherical morphology with diameters predominantly ranged from 80 nm to 250 nm, similar to those previously described OMVs from Gram-negative bacteria [18-20]. We then labeled *S. elongatus*-EVs with a green fluorescent dye (PKH67) and then assessed whether these EVs can be internalized into HMECs. Fluorescence microscopy analysis showed that when the labeled *S. elongatus*-EVs were added to the culture medium of HMECs for 3 h, they were taken up and transferred to

the perinuclear region of HMECs (**Figure 4C**), which confirmed their internalization by HMECs. CCK-8 analysis (**Figure 4D**), transwell migration assay (**Figure 4E-F**), scratch wound healing assay (**Figure 4G-H**) and tube formation assay (**Figure 4I-J**) revealed that direct treatment with *S. elongatus*-EVs significantly enhanced the proliferation, migration and tube formation of HMECs, respectively. Collectively, the above data suggest that EVs play an essential role in *S. elongatus* PCC 7942-induced promotion of angiogenesis of endothelial cells.

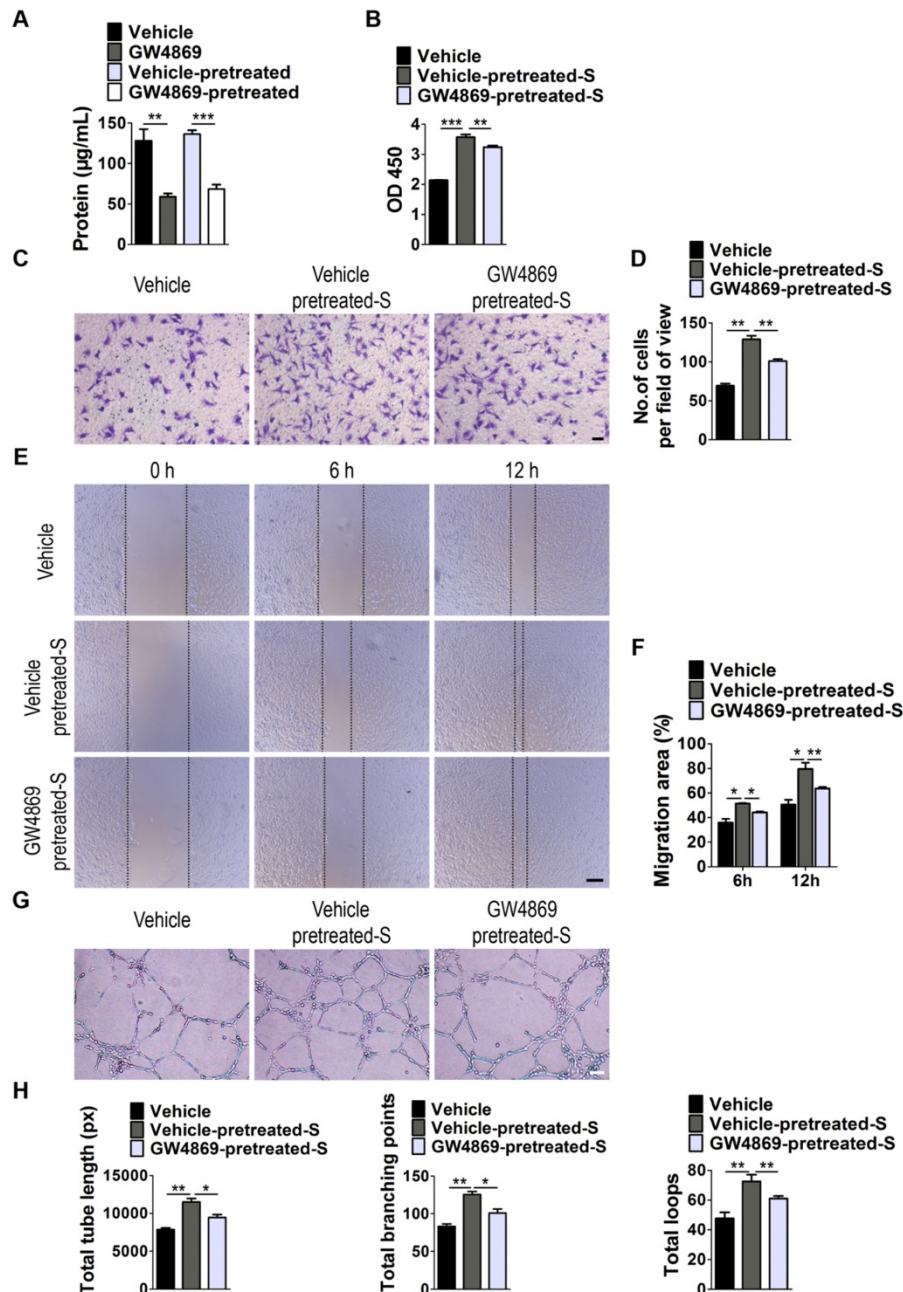


Figure 3. EVs secretion is required for the pro-angiogenic effects of *S. elongatus* PCC 7942. (A) Total protein contents of *S. elongatus*-EVs. n = 3 per group. (B) CCK-8 analysis of HMECs' proliferation. n = 4 per group. S: *S. elongatus* PCC 7942. (C-D) Representative images of transwell migration assay in HMECs (C) and quantitative analysis of the migrated cells (D). Scale bar: 100 µm. n = 3 per group. (E-F) Representative images (E) and quantification (F) of wound healing assay for HMECs. Scale bar: 200 µm. n = 3 per group. (G-H) Representative images (G) and quantification (H) of HMECs' tube formation. Scale bar: 200 µm. n = 3 per group. Data are plotted as mean ± SD. *P < 0.05, **P < 0.01, ***P < 0.001.

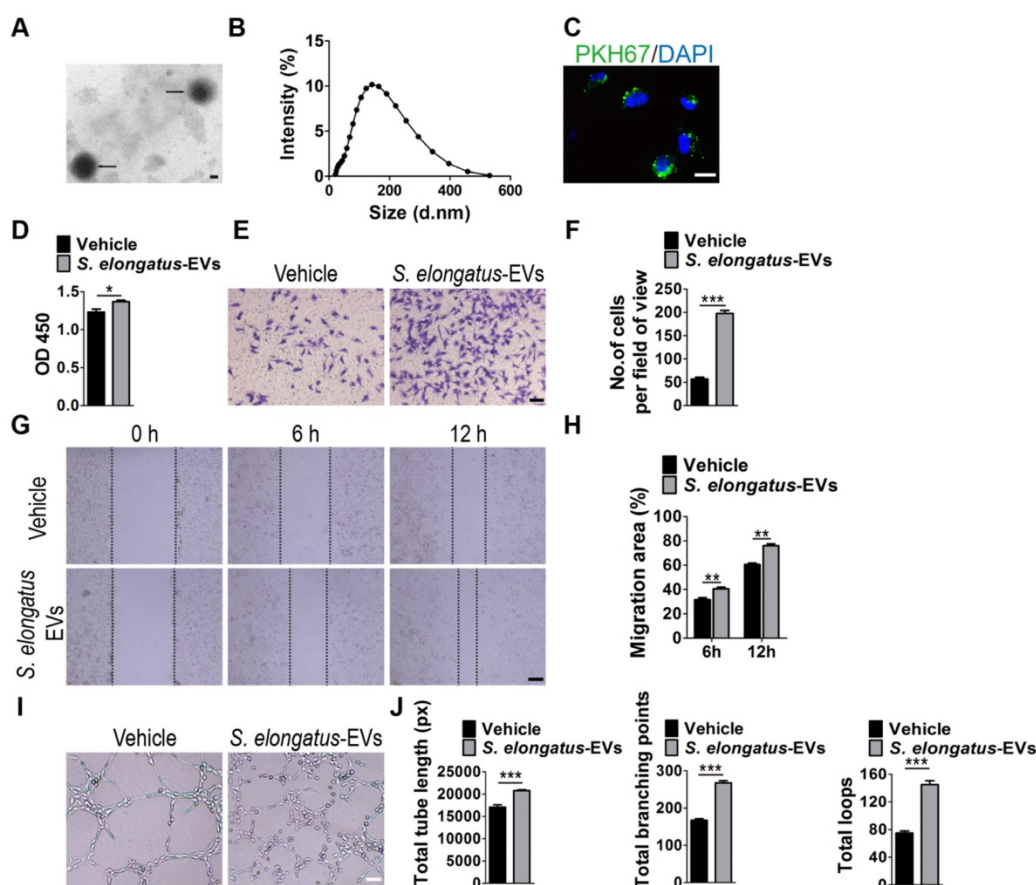


Figure 4. *S. elongatus*-EVs augment the angiogenic activities of endothelial cells. **(A)** Morphology of *S. elongatus*-EVs under transmission electron microscopy. Scale bar: 50 nm. **(B)** Size distribution analysis of *S. elongatus*-EVs by dynamic light scattering. **(C)** Fluorescence microscopy analysis of the internalization of PKH67-labeled *S. elongatus*-EVs by HMECs. Scale bar: 50 μ m. **(D)** CCK-8 analysis of HMECs' proliferation. $n = 4$ per group. **(E-F)** Representative images of transwell migration assay in HMECs **(E)** and quantitative analysis of the migrated cells **(F)**. Scale bar: 100 μ m. $n = 3$ per group. **(G-H)** Representative images **(G)** and quantification **(H)** of wound healing assay for HMECs. Scale bar: 200 μ m. $n = 3$ per group. **(I-J)** Representative images **(I)** and quantification of HMECs' tube formation **(J)**. Scale bar: 200 μ m. $n = 3$ per group. Data are plotted as mean \pm SD. * $P < 0.05$, ** $P < 0.01$, *** $P < 0.001$.

We also investigated the impact of *S. elongatus*-EVs on function properties of human keratinocytes and fibroblasts. As indicated by CCK-8 analysis (Figure S2A) and scratch wound healing assay (Figure S2B-E), stimulation with *S. elongatus*-EVs resulted in decreased proliferation and migration of HSFs, as well as increased migration of HaCaT, which were consistent with the effects of their parent cell *S. elongatus* PCC 7942 and further implied the mediator role of EVs in *S. elongatus* PCC 7942' function. No significant difference was observed in proliferative ability between *S. elongatus*-EVs- and vehicle-treated HaCaT (Figure S2A), which was inconsistent with the inhibitory effects of *S. elongatus* PCC 7942 on the proliferation of HaCaT. Thus, EVs mediate, but not completely, the functions of *S. elongatus* PCC 7942.

The effects of *S. elongatus*-EVs and their parent cell *S. elongatus* PCC 7942 on the proliferation and migration of mouse epidermal JB6 cells and NIH3T3 embryonic fibroblasts were also assessed. CCK-8 analysis showed that both *S. elongatus* PCC 7942 and *S. elongatus*-EVs markedly reduced the proliferation of

JB6 cells (Figure S3A). Although *S. elongatus* PCC 7942 and its EVs statistically significantly suppressed the proliferation of HSFs, no significant changes in proliferation of NIH3T3 mouse fibroblasts were observed after treatment with *S. elongatus* PCC 7942 or its EVs (Figure S3A). Scratch wound healing assay revealed that *S. elongatus* PCC 7942 and *S. elongatus*-EVs could markedly enhance the migration of JB6 cells (Figure S3B-C) and suppress the migration of NIH3T3 mouse fibroblasts (Figure S3D-E), consistent with their potent pro-migratory effects on human keratinocytes and anti-migratory effects on human fibroblasts.

***S. elongatus*-EVs accelerate the healing of cutaneous burn wounds**

We then aimed to confirm the pro-wound healing effects of *S. elongatus*-EVs *in vivo*. Acute burn injuries were established in mice as above described and the wounds were subcutaneously injected with *S. elongatus*-EVs (100 μ g in 100 μ L PBS), *S. elongatus* PCC 7942 (10⁵ cells in 100 μ L PBS) or an equal volume of PBS. All the mice were kept under standard

laboratory condition (12 h light/dark cycles) after injection. As shown in **Figure 5A-B**, similar to the mice treated with *S. elongatus* PCC 7942, wound closure in mice receiving treatment of *S. elongatus*-EVs was also significantly accelerated than that of PBS-treated group. Histological analysis by H&E staining indicated that *S. elongatus*-EVs induced comparable beneficial effects on dermal and epidermal regeneration and inhibitory effects on scar formation relative to their parent cell *S. elongatus* PCC 7942 (**Figure 5C-D**). Masson's trichrome staining

showed that *S. elongatus*-EVs did not induce obvious changes in collagen deposition in the wound sites, similar to those observed in *S. elongatus* PCC 7942 group (**Figure 5E-F**). Ki67 staining revealed that skin cell proliferation in mice transplanted with either *S. elongatus*-EVs or their parent cell *S. elongatus* PCC 7942 was both remarkably enhanced than that of PBS-treated control wounds (**Figure 5G-H**). These data suggest direct transplantation of a certain amount of *S. elongatus*-EVs is sufficient to accelerate the healing of burn wounds.

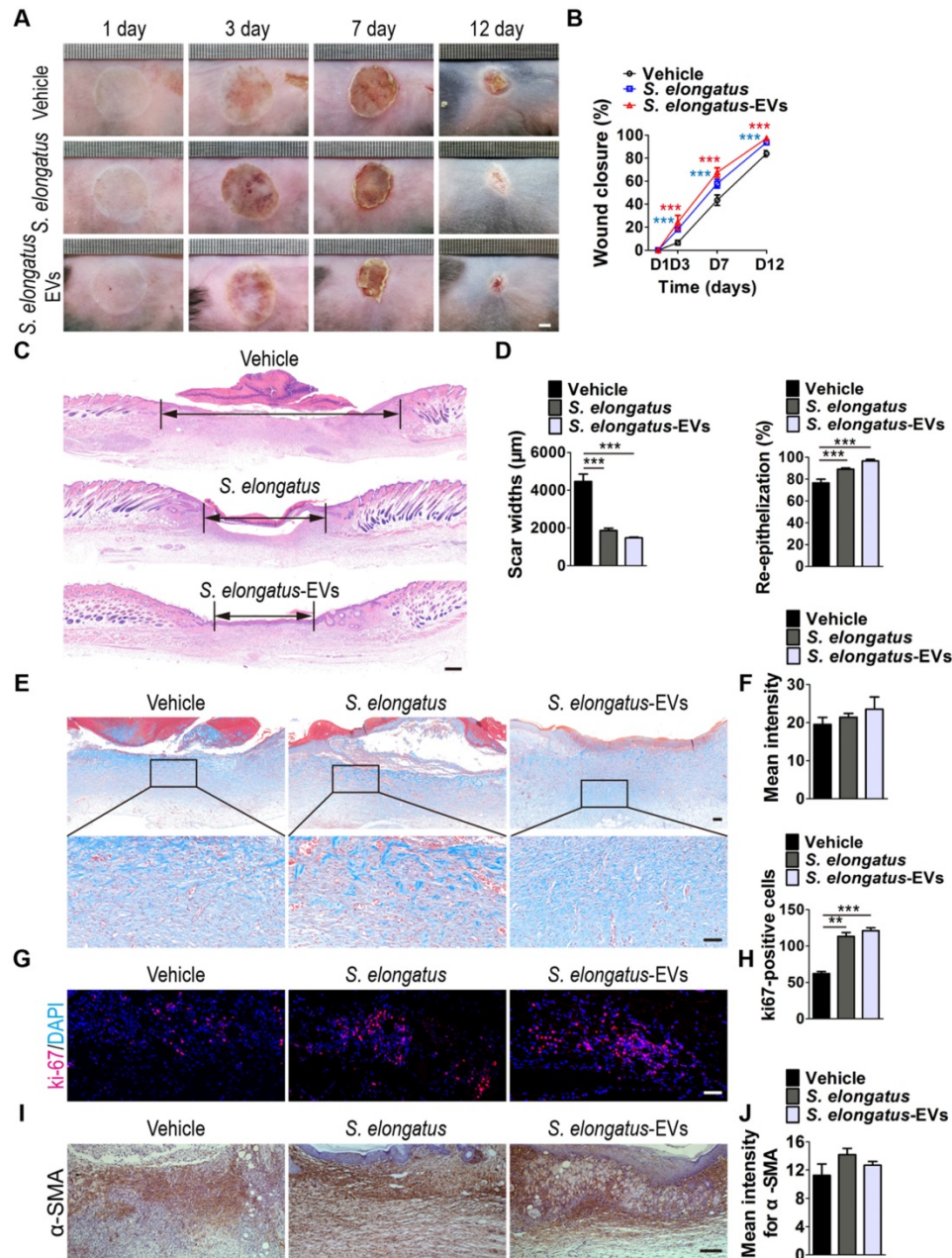


Figure 5. *S. elongatus*-EVs accelerate the healing of cutaneous burn wounds. (A-B) Representative images (A) and closure rate (B) of wounds treated with PBS, *S. elongatus* and *S. elongatus*-EVs at days 3, 7 and 12 post-wounding. Scale bar: 2 mm. n = 10 per group. (C) Representative images of H&E-stained wound sections at day 12 post-wounding. Scale bar: 500 μm. (D) Quantification of the rate of re-epithelialization and scar widths. n = 3 per group. (E) Representative images of Masson's trichrome stained-wound sections at day 12 post-wounding. Scale bar: 100 μm (top) or 50 μm (bottom). (F) Quantification of the mean intensity of Masson's trichrome stained areas. n = 3 per group. (G-H) Representative images (G) and quantification (H) of skin cell proliferation by ki67 immunofluorescence staining. Scale bar: 50 μm. n = 3 per group. (I) Representative images of immunohistochemistry staining for α-SMA. Scale bar: 100 μm. (J) Quantitative analysis of the mean intensity for the α-SMA positively stained areas. n = 3 per group. Data are plotted as mean ± SD. *P < 0.05, **P < 0.01, ***P < 0.001.

During the remodeling phase of wound healing, fibroblasts secrete and reorganize the collagen matrix, transform into myofibroblasts and participate in wound contraction [25]. Immunohistochemistry staining was performed to assess the expression of α -smooth muscle actin (α -SMA), a marker of myofibroblastic differentiation of dermal fibroblasts. The results revealed that *S. elongatus* PCC 7942 and *S. elongatus*-EVs induced an increase of α -SMA expression in the burn wound sites of mice at post-wounding day 12, but the differences were not statistically significant (Figure 5I-J).

S. elongatus-EVs enhance angiogenesis in the wound sites

We next determined whether angiogenesis in the wound sites is enhanced after *S. elongatus*-EVs transplantation. As evidenced by the gross view of skin tissues from the undersurface (Figure 6A) and CD31 immunostaining (Figure 6B-C), the wounds treated with *S. elongatus*-EVs, similar to that of wounds receiving *S. elongatus* PCC 7942 therapy, had significantly more blood vessel formation compared with the PBS- treated control wounds. These data

suggest that *S. elongatus*-EVs can be directly used for therapeutic angiogenesis to expedite wound healing.

We compared the growth state of endothelial cells treated with *S. elongatus* PCC 7942 and their EVs and found that endothelial cells directly exposed to *S. elongatus* PCC 7942 showed dose-dependent morphological changes compared to the control cells (Figure S4A). The normal endothelial cells exhibited even edges and a smooth surface, but the surface of the high concentration of *S. elongatus* PCC 7942-treated cells became rough and their intracellular organelles appear fuzzy and hard to distinguish (Figure S4A). Although *S. elongatus* PCC 7942 treatment induced a dose-dependent increase of the proliferation of endothelial cells at the concentration from 10^5 to 10^7 cells/mL, higher numbers of *S. elongatus* PCC 7942 indeed had a serious bad impact on the growth of endothelial cells, as indicated by CCK-8 assay (Figure S4A-B). However, *S. elongatus*-EVs did not affect the morphology and growth state of endothelial cells, even used at a very high concentration (Figure S4A-B). Thus, direct use of *S. elongatus*-EVs may avoid some bad effects of exposure to *S. elongatus* PCC

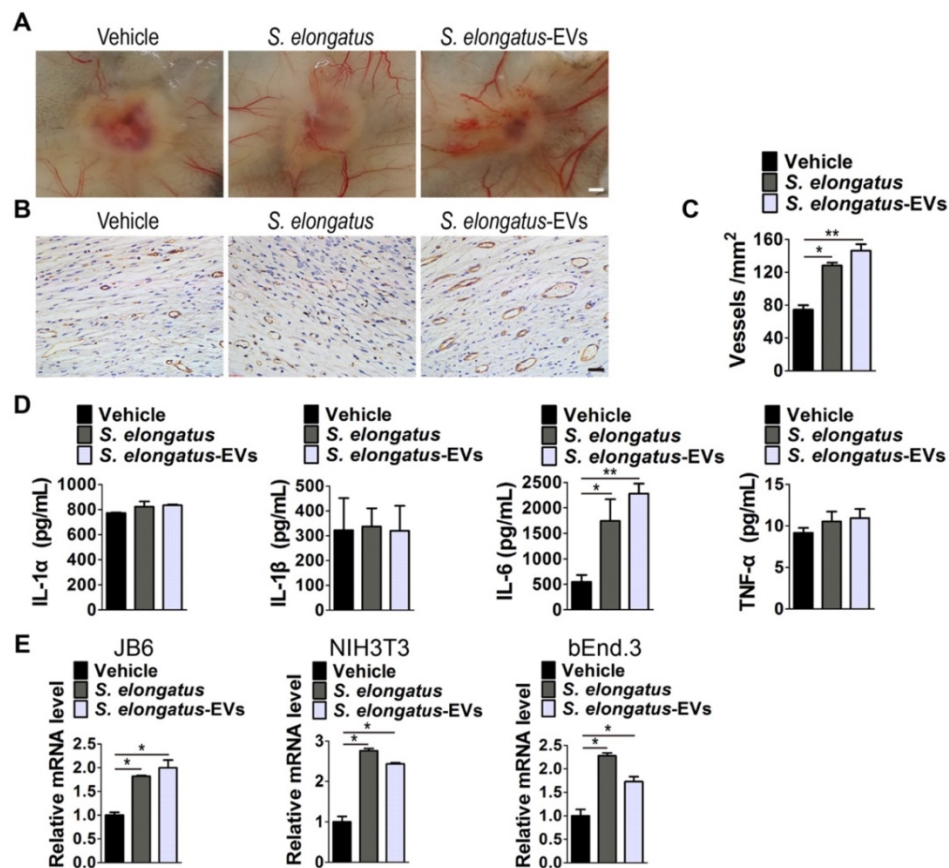


Figure 6. *S. elongatus*-EVs enhance angiogenesis in the wound sites and IL-6 expression *in vivo* and *in vitro*. (A) Gross view of wounds treated with vehicle (PBS), *S. elongatus* and *S. elongatus*-EVs at day 12 post-wounding from the undersurface. Scale bar: 2 mm. (B-C) Representative images (B) and quantification (C) of CD31-stained blood vessels in the wound sites. Scale bar: 50 μ m. n = 3 per group. (D) ELISA of the concentrations of IL-1 α , IL-1 β , IL-6 and TNF- α in skin tissue homogenate from mice treated with vehicle, *S. elongatus* and *S. elongatus*-EVs at day 7 post-wounding. n = 3 per group. (E) qRT-PCR analysis of the expression levels of IL-6 in mouse epidermal JB6 cells, NIH3T3 fibroblasts and bEnd.3 endothelial cells receiving different treatments for 24 h. n = 3 per group. Data are plotted as mean \pm SD. * P < 0.05, ** P < 0.01, *** P < 0.001.

7942, which further suggests the superiority of *S. elongatus*-EVs for therapeutic purposes.

S. elongatus*-EVs enhance interleukin 6 (IL-6) expression *in vivo* and *in vitro

We then assessed the levels of a class of pro-inflammatory cytokines including IL-1 α , IL-1 β , IL-6 and tumor necrosis factor α (TNF- α), which have regulatory roles in wound healing [26-31]. As evidenced by ELISA test for skin tissue homogenate from mice treated with *S. elongatus* PCC 7942, *S. elongatus*-EVs or vehicle for 7 days, *S. elongatus* PCC 7942 and its EVs did not induce notable changes of expression of IL-1 α , IL-1 β and TNF- α , but induced a significant increase of IL-6 expression in the wounds (**Figure 6D**). We further tested IL-6 expression in mouse epidermal JB6 cells, NIH3T3 fibroblasts and brain microvascular endothelial cell line bEnd.3 treated with *S. elongatus* PCC 7942, *S. elongatus*-EVs or vehicle (PBS) for 24 h. Quantitative real-time PCR (qRT-PCR) analysis showed that both *S. elongatus* PCC 7942 and its EVs were able to induce a prominent increase of IL-6 mRNA expression in JB6, NIH3T3 and bEnd.3 cells (**Figure 6E**). Since IL-6 plays an essential role in angiogenesis during skin wound healing [29], our findings suggest that the promotion of IL-6 expression by endothelial cells, epidermal cells and fibroblasts in the wound sites may be a mechanism by which *S. elongatus* PCC 7942 and *S. elongatus*-EVs augment angiogenesis and accelerate the healing process of burn wounds.

Discussion

Poor wound healing after surgery, trauma, acute illness, or chronic disease conditions affects millions of people worldwide each year [32]. Various kinds of therapies have been attempted to speed up the wound healing process, but the optimal strategies are still being developed [17]. In this study, we provide evidence that local transplantation of *S. elongatus* PCC 7942, a naturally occurring cyanobacterium that can be easily obtained and large-scale expanded under the condition of light, CO₂ and low nutrients [10], can accelerate the healing process of acute cutaneous burn wounds in mice. During the process of *S. elongatus* PCC 7942-induced promotion of wound healing, the augmentation of angiogenic responses of endogenous endothelial cells may play a crucial role, as the wounds treated with the cyanobacteria have greater new blood vessel formation and incubation with the cyanobacteria increases the proliferation, migration and tube formation of endothelial cells *in vitro*. The inhibitory effects of *S. elongatus* PCC 7942 on the proliferation of keratinocytes and fibroblasts as well as on the migration of fibroblasts further suggest that

its pro-wound healing action is not exerted primarily by direct activation of these two types of wound healing-related cells. Our data suggest that *S. elongatus* PCC 7942 enhance the angiogenic activities of endothelial cells in the wound sites, thereby facilitating dermal and epidermal repair and regeneration.

S. elongatus PCC 7942 has the ability to consume carbon dioxide and produce oxygen by photosynthesis after light exposure. Cohen et al recently placed both this photoautotroph and mouse cardiomyocytes together and found that this treatment induces a substantial increase in oxygen tension and enhances cellular metabolism of cardiomyocytes [11]. Then, they took a bold step to test if application of *S. elongatus* PCC 7942 in live animals can provide oxygen to the ischemic myocardium. The results revealed that intramyocardial injection of *S. elongatus* PCC 7942 into the rat ischemic heart enhances tissue oxygenation and provides long-term functional benefit as a result of short-term light exposure (approximately 2 h) [11]. An inadequate supply of oxygen due to blood vessel damage is a major contributor to delayed wound healing [33]. In our study, we initially attempted to investigate the therapeutic efficacy of such a photosynthetic therapy in mouse skin wound healing. However, we found that the wounds receiving *S. elongatus* PCC 7942 injections either in the light or in the darkness both exhibit much more new vessel formation and much faster wound closure relative to the control wounds. *In vitro* functional assays also showed that the regulatory effects of the cyanobacteria on wound healing-related cells (including keratinocytes, fibroblasts and endothelial cells) do not appear to be dependent on its active photosynthesis, as the photoautotroph was just cultured with the recipient cells in a standard carbon dioxide cell incubator without being given the extra light as soon as it was added to the cultures of the recipient cells. Thus, the therapeutic effects of *S. elongatus* PCC 7942 can be exerted without the need for the cells or tissues to be in direct light. It should be noted that the results of the study by Cohen et al showed that *S. elongatus* PCC 7942 therapy in the dark also induces a nearly 30% increase in cardiac output in rat with myocardial ischemia compared to the ischemic control [11], which further implies that *S. elongatus* PCC 7942 is able to exert beneficial effects through some mechanisms independent of light-dependent photosynthesis.

The most important findings of our study are that EVs secretion is required for *S. elongatus* PCC 7942-induced promotion of endothelial angiogenesis and direct local transplantation of these EVs (*S.*

elongatus-EVs) can efficiently enhance the formation of blood vessels and expedite the healing of burn wounds in mice. In recent years, EVs-based cell-free therapy has become a very attractive alternative for regenerative medicine, due to EVs' advantages of non-tumorigenicity, low immunogenicity, high stability, ease of reaching the wound sites and no vascular obstructive concern relative to cell-based therapy [15-17, 34]. For *S. elongatus* PCC 7942, except for the above considerations, direct application of *S. elongatus*-EVs rather than the cyanobacteria themselves for therapeutic uses can avoid potential biohazards. Cohen et al showed that the cyanobacteria do not affect the survival of cardiomyocytes *in vitro* and local injection of the cyanobacteria into the rat heart does not elicit a meaningful pathologic immune response [11]. In our study, however, we found that treatment with high concentrations of *S. elongatus* PCC 7942 results in morphological changes and growth inhibition of cultured endothelial cells, suggesting that exposure to excessive *S. elongatus* PCC 7942 can cause considerable toxicities to the recipient cells. Thus, although the study by Cohen et al showed that the persistence of the cyanobacteria in the tissue is likely short-lived, with most of the local injected cells cleared from the tissue by 24 h [11], it is still hard to guarantee that the cyanobacteria do not survive and proliferate in large quantities to injure the recipient tissues under any circumstances. Fortunately, we found that their EVs not only mediate the pro-angiogenic and -wound healing effects of the cyanobacteria, but also show no obvious toxicities to the recipient cells even used at very high concentrations, suggesting a more promising prospect of clinical utilization of *S. elongatus*-EVs for the acceleration of wound healing. The effects of *S. elongatus*-EVs on recipient cells are similar, but not entirely consistent with those of their parent cell *S. elongatus* PCC 7942, suggesting that the regulation of *S. elongatus* PCC 7942 is a result of the combination of various factors and EVs just mediate partial functions of the cyanobacteria.

A limitation of our study is that we did not identify the molecular mechanism by which *S. elongatus*-EVs exert their pro-angiogenic and -wound healing function. The molecules that mediate the different effects of *S. elongatus*-EVs on the proliferation and migration of endothelial cells, keratinocytes and fibroblasts also remain unclear. It has been established that EVs can serve as vehicles to transfer bioactive lipids, nucleic acids and proteins to target cells to regulate their biological responses [12]. We recently demonstrated that EVs from human urine-derived stem cells can enhance angiogenic

activities of endothelial cells via transferring a pro-angiogenic protein called deleted in malignant brain tumors 1 (DMBT1) [17]. Vanaja et al reported that EVs from enterohemorrhagic *Escherichia coli* are able to deliver lipopolysaccharide (LPS) into the cytosol of host cells to trigger cell death [20]. Thus, *S. elongatus*-EVs may also be selectively enriched in some functional molecules that mediate their regulatory effects, which require further exploration.

In the recipient cells and tissues, we found that both *S. elongatus*-EVs and their parent cell *S. elongatus* PCC 7942 could induce a marked increase of IL-6 expression in cultured endothelial cells, epidermal cells and fibroblasts as well as mouse wounded tissues. IL-6 expression is reported to be induced by skin injury and IL-6-deficient mice display delayed angiogenesis and wound healing, which can be reversed by IL-6 overexpression [28, 29]. These findings, along with the potent pro-angiogenic effects of *S. elongatus* PCC 7942 and *S. elongatus*-EVs *in vivo* and *in vitro*, suggest that the promotion of IL-6 expression may be a mechanism by which *S. elongatus* PCC 7942 and its EVs augment angiogenesis and accelerate the healing process of burn wounds. However, the role of IL-6 in these processes is not further determined in the present study and still needs further determination.

In summary, our data suggest that *Synechococcus elongatus* PCC 7942 secretes EVs to evoke the angiogenic responses of endothelial cells, thereby facilitating cutaneous wound repair and regeneration. Nevertheless, it should be noted that *S. elongatus* PCC 7942 and its EVs may also regulate other wound healing-related process, such as wound contraction. Although *S. elongatus* PCC7942 and its EVs just induced a trend increase of expression of α -SMA, the main functional marker of myofibroblastic differentiation and contractility [35] in the mouse wound sites on post-burn day 12, the cyanobacterium and its EVs might have the ability to stimulate the contraction of wound at the early phase of wound healing. The expression of α -SMA in the mouse burn wounds receiving *S. elongatus* PCC7942, *S. elongatus*-EVs or vehicle treatments at the early stage of wound healing was not assessed in the present study. Future studies are required to determine the effects of *S. elongatus* PCC7942 and *S. elongatus*-EVs on wound contraction and the underlying molecular mechanism.

Materials and Methods

Cell culture

S. elongatus PCC 7942 was purchased from the Freshwater Algae Culture Collection at the Institute of

Hydrobiology (FACHB-805; Chinese Academy of Sciences, Wuhan, China). The cyanobacteria were incubated in BG-11 liquid medium (GIBCO-BRL Life Technologies, Grand Island, USA) in 250-mL flasks. The culture was placed on a shaker (MaxQ 2000, Thermo Fisher Scientific Inc.) rotating at 125 rpm in a 30 °C incubator illuminated with two 18-inch plant fluorescent light bulbs (Shunde POVI Biological Technology, Guangdong, China). Fresh BG-11 medium was added daily to the culture to maintain a constant volume. Every four days, approximately 25% of the cyanobacteria was discarded and replaced with an equal volume of fresh BG-11 medium.

HaCaT (FuHeng Biology, Shanghai, China), HSFs (FuHeng Biology), JB6 cells (Zhong Qiao Xin Zhou Biotechnology, Shanghai, China), NIH3T3 cells (Cyagen Biosciences, Guangzhou, China) and bEnd.3 cells (UCbio, Changsha, China) were cultured in high-glucose Dulbecco's modified eagle medium (DMEM; Gibco) containing 10% fetal bovine serum (FBS; Gibco). Human microvascular endothelial cells (HMECs; Cell Bank of the Chinese Academy of Sciences, Shanghai, China) were incubated in MCDB131 culture medium (Gibco) supplemented with 10% FBS (Gibco) and 1% GlutaMAX (Gibco). Cultures were maintained at 37 °C and 5% CO₂ in a humidified atmosphere.

Isolation and identification of *S. elongatus*-EVs

S. elongatus-EVs were isolated from *S. elongatus* PCC 7942 cultures (24 h of growth) by differential centrifugation. Briefly, the cyanobacteria were pelleted at 10,000 × g for 5 min and the conditioned medium was collected and centrifuged at 4,000 × g for 30 min to remove dead cells and cellular debris. The supernatant was filtered using a 0.45 μm filter (Millipore, Billerica, USA) and centrifuged at 10,000 × g for 30 min to further remove debris, followed by ultracentrifugation for 60 min at 100,000 × g. The pelleted EVs were washed with 15 mL of PBS, centrifuged at 100,000 × g for 60 min and then re-suspended in 15 mL of PBS. The EVs suspension was filtered through a 0.22 μm filter (Millipore), transferred to an Amicon Ultra-15 Centrifugal Filter Unit (100 kDa; Millipore) and concentrated to about 1 mL by centrifugation at 4000 × g. All procedures were performed at 4 °C. The protein content of *S. elongatus*-EVs was assessed by a Pierce bicinchoninic acid (BCA) Protein Assay Kit (Thermo Fisher Scientific, USA). *S. elongatus*-EVs were stored at -80 °C or used for the downstream assays. The morphology of *S. elongatus*-EVs was observed by a transmission electron microscope (Hitachi, Tokyo, Japan) and the size distribution of *S. elongatus*-EVs was measured by dynamic light scattering with a Nanosizer™

instrument (Malvern Instruments, Malvern, UK) as described previously in detail [2, 36].

Mouse burn wound model and treatments

Three months old female C57BL/6 mice weighing 25-30 g were used in the present study. All animal care and experimental procedures were approved by the Laboratory Animal Management Committee of Xiangya Hospital of Central South University. The mice were anesthetized by intraperitoneal injection of 50 mg/kg pentobarbital sodium (Sigma-Aldrich, St. Louis MO, USA). A metal rod (25 g, 1 cm in diameter) was heated to 95-100°C by submersion in boiling water. After shaving the mice, the rod was immediately positioned vertically for 6 seconds on the upper back skin of mice without additional pressure. Two full-thickness burn wounds were created on each mouse. After wounding, the mice were received the following treatments and the wounds were not dressed.

To investigate whether *S. elongatus* PCC 7942 can provide therapeutic benefits to mouse burn wounds, animals (n = 5 per group) were randomized to receive subcutaneously injections of *S. elongatus* PCC 7942 (10⁵ cells in 100 μL PBS) in the light (*S. elongatus*-light), *S. elongatus* PCC 7942 (10⁵ cells in 100 μL PBS) in the dark (*S. elongatus*-dark) or an equal volume of vehicle control (PBS) at 4 injection sites (25 μL per site). The treatments were conducted only at day 0 and day 5 post-wounding. For experiments in the light, injection syringes containing *S. elongatus* PCC 7942 were kept in the incubator under plant lights for 2 h after preparation. For experiments in the dark, samples were placed in opaque black bags to prevent light exposure (approximately 2 h). In the *S. elongatus*-light and control groups, the wounds were exposed to light during injection and the mice were kept under standard laboratory condition (12 h light/dark cycles) after injection. In the *S. elongatus*-dark groups, room lights were turned off during injection and only the minimum amount of indirect light needed by the researcher to see the burned area was used. After injection, several layers of aluminum foil were placed over the cages to prevent the wounds from light exposure. After 24 h, the mice in the dark groups were also kept under standard laboratory condition (12 h light/dark cycles). To test the effects of *S. elongatus*-EVs on wound healing, the mice were randomly divided into 3 groups (n = 5 per group) and subcutaneously injected with *S. elongatus*-EVs (100 μg in 100 μL PBS), *S. elongatus* PCC 7942 (10⁵ cells in 100 μL PBS) or PBS alone at day 0 and day 5 post-wounding. Preparation and injection were performed under normal room light and the mice were kept under standard laboratory condition (12 h

light/dark cycles) after injection. At day 3, 7, and 12 post-wounding, all the wounds were photographed and measured with a caliper rule. The rate of wound closure was calculated using the equation as previously described [17]: wound closure (%) = $(A_0 - A_t)/A_0 \times 100$, where A_0 is the initial wound area, and A_t is the wound area at the indicated times. At day 12 post-wounding, the mice were sacrificed and skin samples containing the wound bed and surrounding healthy skin tissues were harvested. The undersurface of the skin was photographed to detect the newly formed blood vessels. The skin samples were then processed for histological, immunohistochemistry and immunofluorescent analyses.

To detect the protein expression of IL-1 α , IL-1 β , IL-6 and TNF- α , the mice (n = 3 per group) were treated with *S. elongatus* PCC 7942, *S. elongatus*-EVs or an equal volume of vehicle (PBS) as described above and the mice were killed at post-wounding day 7. Skin samples containing the wound bed and surrounding healthy skin tissues were obtained. Skin tissue homogenate was prepared and the concentrations of IL-1 α , IL-1 β , IL-6 and TNF- α were measured by ELISA according to the manufacturer's instructions (Multi Sciences LTD. (Hangzhou, China).

Histological, immunohistochemistry and immunofluorescent analyses

Skin samples were fixed in 4% paraformaldehyde for 24 h, dehydrated using a series of graded ethanol and embedded in paraffin. Then, the paraffin-fixed specimens were cut into 4- μ m-thick sections, deparaffinized in xylene, rehydrated through decreasing concentrations of ethanol to distilled water, and then subjected to histological analysis, immunohistochemistry and immunofluorescent staining.

For histological analysis, the rehydrated sections were stained with hematoxylin and eosin (H&E) (Servicebio, Wuhan, China) or Masson's trichrome (Servicebio). Width of the scar and length of the neoeppithelium were measured on H&E-stained sections. The re-epithelialization rate (E%) was assessed using the equation: $E\% = W_n/W_o \times 100$, where W_o is the distance between original wound bed and W_n is the length covered by neoeppithelium. The mean intensity for Masson-stained areas was measured in three random visual fields per section using Image-Pro Plus 6 software.

For immunohistochemistry (IHC) staining for CD31 and α -SMA, the rehydrated sections were heated in EDTA-Tris buffer (pH 9.0) in a microwave for 15 min to retrieve the antigen. Endogenous peroxidase was blocked by 3% hydrogen peroxide (H_2O_2) for 25 min. Then, the sections were blocked

with 3% bovine serum albumin (BSA; Servicebio) for 30 min and incubated with the primary antibody anti-CD31 (1:50; Abcam) or anti- α -SMA (1:1000; Abcam) overnight at 4°C. A horseradish peroxidase IHC detection system (Servicebio) was used to detect the immunoactivity, followed by counterstaining with hematoxylin. The sections were viewed under an optical microscope (CX31; Olympus, Hamburg, Germany). The numbers of CD31-positive vessels and mean intensity for α -SMA-positive areas were quantified in three random visual fields per section.

For immunofluorescence staining for ki67, after antigen retrieval by boiling in EDTA-Tris buffer (pH 9.0), sections were incubated with spontaneous fluorescence quenching agent (Servicebio) for 5 min, blocked with 3% BSA at room temperature for 30 min and then incubated with the primary antibody anti-ki67 (1:100; Abcam, Cambridge, Britain) overnight at 4°C. After washing three times with PBS, sections were incubated with the secondary antibody (1:250; Abcam) at room temperature for 50 min while avoiding light. Nuclei were stained with DAPI (0.5 μ g/mL; Invitrogen, Carlsbad, USA). The signals were examined with a fluorescence microscope (Leica DMI6000B, Solms, Germany). Ki67-positive cells were quantified from three random visual fields per section.

Exosomes uptake assay

S. elongatus-EVs were labeled with the green fluorescent membrane tracer PKH67 (Sigma) according to the manufacturer's protocol. After 5 min of incubation with the PKH67 dye solution at room temperature, the mixture was transferred to an Amicon Ultra-15 Centrifugal Filter Unit (100 kDa; Millipore) and washed twice with PBS by centrifugation (4000 \times g for 30 min). Next, *S. elongatus*-EVs were incubated with HMECs at 37 °C for 3 h. The treated cells were then washed with PBS and fixed in 4% paraformaldehyde for 15 min. After washing twice with PBS, cells were stained with DAPI (Invitrogen) and observed using a fluorescence microscope (Leica).

Inhibition of EVs secretion

To verify the ability of GW4869 to inhibit EVs secretion by *S. elongatus* PCC 7942, the cyanobacteria were treated with GW4869 (10 μ M; Santa Cruz Biotechnology, Santa Cruz, USA) or an equal volume of vehicle dimethyl sulfoxide (DMSO) for 24 h. Then, their conditioned media were harvested for isolation of EVs. Fresh medium was added to these cyanobacteria, which continued to grow for another 24 h. The conditioned medium of these cyanobacteria was also collected for EVs isolation. The protein

content of the isolated EVs was measured with a BCA Protein Assay Kit (Thermo Fisher Scientific). To test the role of EVs in *S. elongatus* PCC 7942-induced regulation of endothelial cell function, the cyanobacteria was pre-treated with GW4869 or vehicle for 24 h. These GW4869-pretreated cyanobacteria were used to co-culture with HMECs for downstream functional assays.

CCK-8 proliferation assay

For CCK-8 assay, cells were seeded at 5×10^3 cells per well (four replicates per group) into 96-well culture plates and treated with GW4869-pretreated or un-treated *S. elongatus* PCC 7942 (10^6 cells/mL), *S. elongatus*-EVs (100 µg/mL) or an equal volume of vehicle (PBS) for 24 h. The culture medium was then removed and replaced with fresh medium (100 µL per well). CCK-8 reagent (10 µL per well; 7Sea Biotech, Shanghai, China) was added to the medium and the cultures were incubated at 37 °C for 3 h. A group without cells served as the blank. The absorbance was read at 450 nm using a Bio-Rad 680 microplate reader (Bio-Rad, Hercules, USA). Cell proliferation was represented by the optical density calculated from the mean absorbance value of each group minus the mean value of the blank control wells.

Scratch wound healing assay

For scratch wound healing assay, cells were seeded at 2×10^5 cells per well (three replicates per group) into a 12-well plate and kept in an incubator under 5% CO₂ at 37 °C. 12 h later, the monolayer was scratched using a sterile p200 pipette tip and washed with PBS to remove unattached cells. Then, the attached cells were treated with GW4869-pretreated or un-treated *S. elongatus* PCC 7942 (10^6 cells/mL), *S. elongatus*-EVs (100 µg/mL) or an equal volume of PBS. Mitomycin-C (5 µg/mL; Sigma) was present throughout the wound healing assays to avoid the interference of cell proliferation on wound closure. HaCaT cells were photographed at 0 h, 12 h and 48 h post-wounding and HMECs were photographed at 0 h, 6 h and 12 h post-wounding. The migration rate was assessed by calculating the ratio of closure area at the indicated times to initial wound as described previously [17].

Transwell migration assay

Cell migration was measured in a Boyden chamber using 24-well transwell inserts with 8 µm pore-sized filters (Corning, NY, USA) as described previously [17]. Briefly, cells were seeded at a density of 1×10^4 cells per well (three replicates per group) into the upper chamber. The lower chamber was added with 500 µL of complete medium supplemented with GW4869-pretreated or un-treated

S. elongatus PCC 7942 (10^6 cells/mL), *S. elongatus*-EVs (100 µg/mL) or an equal volume of PBS. 12 h later, unigrated cells that remained on the upper surface of the filter were removed by cotton swabs and the migrated cells on the bottom side of the filter were stained with 0.5% crystal violet solution for 20 min. The number of migrated cells was counted under an optical microscope (Leica).

Tube formation assay

For tube formation assay, 50 µL of thawed Matrigel per well was coated onto wells of a pre-cooled 96-well plate and incubated for 30 min at 37 °C. Then, cells were seeded at 2×10^4 cells per well (three replicates per group) into the Matrigel-coated plates and exposed to GW4869-pretreated or un-treated *S. elongatus* PCC 7942 (10^6 cells/mL), *S. elongatus*-EVs (100 µg/mL) or an equal volume of PBS. After 6 h of incubation, tube formation was examined under an inverted microscope (Leica). Tube formation was quantitated by counting the total branching points, total tube length and total loops using Image-Pro Plus 6.0 software.

qRT-PCR analysis

TRIzol Reagent (Invitrogen) was used to extract total RNA from cells treated with *S. elongatus* PCC 7942 (10^6 cells/mL), *S. elongatus*-EVs (100 µg/mL) or an equal volume of PBS for 24 h. cDNA was synthesized using 1 µg of total RNA with a RevertAid First Strand cDNA Synthesis kit (Fermentas, Burlington, Canada) and then amplified on an ABI PRISM® 7900HT System (Applied Biosystems, Foster City, USA) with FastStart Universal SYBR Premix ExTaq™ II (Takara Biotechnology, Japan). The $2^{-\Delta\Delta CT}$ method was adopted to calculate the relative gene expression and GAPDH was used as an internal control gene to normalize the expression of target gene. Primer sequences used for qRT-PCR analysis were as follows: *IL-6*: forward, 5'-TAGTCCTCCTA CCCC AATTTC-3', and reverse, 5'-TTGGTCCTAG CCACTCCTTC-3'; *Gapdh*: forward, 5'-CACCATGGA GAAGGCCGGGG-3', and reverse, 5'-GACGGACAC ATTGGGGGTAG-3'.

Statistical analysis

All data are presented as mean ± standard deviation (SD). Statistical analyses were performed using GraphPad Prism 5 software. Comparisons between two groups were analyzed using the unpaired, two tailed Student's *t*-test. Multiple-group comparisons was analyzed by one-way analysis of variance (ANOVA), followed by the Bonferroni post hoc test to determine the significance of differences between two groups. A value of $p < 0.05$ was judged to be statistically significant.

Abbreviations

S. elongates: *Synechococcus elongates*; EVs: extracellular vesicles; OMVs: outer membrane vesicles; *S. elongatus*-EVs: *S. elongatus* PCC 7942-derived EVs; CCK-8: cell counting kit-8; α -SMA: α -smooth muscle actin; qRT-PCR: quantitative real-time polymerase chain reaction; HMECs: human microvascular endothelial cells; HSFs: human skin fibroblasts; IL-6: interleukin (IL-6); TNF- α : tumor necrosis factor α ; DMEM: dulbecco's modified eagle medium; FBS: fetal bovine serum; BCA: bicinchoninic acid; BSA: bovine serum albumin; H&E: hematoxylin and eosin; IHC: immunohistochemistry; H₂O₂: hydrogen peroxide; DMSO: dimethyl sulfoxide; SD: standard deviation; ANOVA: one-way analysis of variance; LPS: lipopolysaccharide; DMBT1: deleted in malignant brain tumors 1.

Supplementary Material

Supplementary figures.

<http://www.thno.org/v09p2678s1.pdf>

Acknowledgements

This work was supported by the Excellent Young Scientist Award of National Natural Science Foundation of China (Grant No. 81522012), the National Natural Science Foundation of China (Grant No. 81670807, 81871822, 81702237, 81600699, 81801395, 81701383, 81802138), the Thousand Youth Talents Plan of China (Grant No. D1119003), the Medicine and Health Science and Technology Innovation Project of Chinese Academy of Medical Sciences (Grant No. 2018-I2M-HL-024), the High Level Talent Gathering Project of Hunan Province (Grant No. 2017XK2039, 2018RS3029), the Innovation Driven Project of Central South University (2016CX028, 2019CX014, 2018CX029), the Youth Foundation of Xiangya Hospital in Central South University (Grant No. 2016Q10), the Fundamental Research Funds for the Central Universities of Central South University (Grant No. 2018zzts895, 2017zzts032, 2017zzts014), the Hunan Province Natural Science Foundation of China (Grant No. 2017JJ3501), the China Postdoctoral Science Foundation (Grant No. 2017M612596, 2017M622614) and the Natural Science Foundation for Distinguished Young Scholars of Guangdong Province (2016A030306051).

Author contributions

HY, YWL, YJT, SSR, MJL, XKH and TY performed the experiments. HX and CYC designed the experiments. HY analysed the data. HY and CYC prepared all the figures. FY, FYH and CW provided *Synechococcus elongatus* PCC7942. ZLD, ZZL, ZXW, JC,

HML, JHL and SYT provided technical support. HX and CYC wrote the manuscript.

Competing Interests

The authors have declared that no competing interest exists.

References

1. He Z, Ong CH, Halper J, Bateman A. Progranulin is a mediator of the wound response. *Nat Med.* 2003; 9: 225-9.
2. Zhang J, Chen C, Hu B, Niu X, Liu X, Zhang G, et al. Exosomes Derived from Human Endothelial Progenitor Cells Accelerate Cutaneous Wound Healing by Promoting Angiogenesis Through Erk1/2 Signaling. *Int J Biol Sci.* 2016; 12: 1472-87.
3. Li WW, Talcott KE, Zhai AW, Kruger EA, Li VW. The role of therapeutic angiogenesis in tissue repair and regeneration. *Adv Skin Wound Care.* 2005; 18: 491-500; quiz 1-2.
4. Liu F, Chen DD, Sun X, Xie HH, Yuan H, Jia W, et al. Hydrogen sulfide improves wound healing via restoration of endothelial progenitor cell functions and activation of angiopoietin-1 in type 2 diabetes. *Diabetes.* 2014; 63: 1763-78.
5. Atsumi S, Higashide W, Liao JC. Direct photosynthetic recycling of carbon dioxide to isobutyraldehyde. *Nat Biotechnol.* 2009; 27: 1177-80.
6. Xu Y, Ma P, Shah P, Rokas A, Liu Y, Johnson CH. Non-optimal codon usage is a mechanism to achieve circadian clock conditionality. *Nature.* 2013; 495: 116-20.
7. Kato A, Takatani N, Ikeda K, Maeda SI, Omata T. Removal of the product from the culture medium strongly enhances free fatty acid production by genetically engineered *Synechococcus elongatus*. *Biotechnol Biofuels.* 2017; 10: 141.
8. Rubin BE, Wetmore KM, Price MN, Diamond S, Shultzaberger RK, Lowe LC, et al. The essential gene set of a photosynthetic organism. *Proc Natl Acad Sci U S A.* 2015; 112: E6634-43.
9. Lan EI, Wei CT. Metabolic engineering of cyanobacteria for the photosynthetic production of succinate. *Metab Eng.* 2016; 38: 483-493.
10. Broddrick JT, Rubin BE, Welkie DG, Du N, Mih N, Diamond S, et al. Unique attributes of cyanobacterial metabolism revealed by improved genome-scale metabolic modeling and essential gene analysis. *Proc. Natl. Acad. Sci. U. S. A.* 2016; 113: E8344-E53.
11. Cohen JE, Goldstone AB, Paulsen MJ, Shudo Y, Steele AN, Edwards BB, et al. An innovative biologic system for photon-powered myocardium in the ischemic heart. *Sci Adv.* 2017; 3: e1603078.
12. S ELA, Mäger I, Breakefield XO, Wood MJ. Extracellular vesicles: biology and emerging therapeutic opportunities. *Nat Rev Drug Discov.* 2013; 12: 347-57.
13. Li Y, Cheng Q, Hu G, Deng T, Wang Q, Zhou J, et al. Extracellular vesicles in mesenchymal stromal cells: A novel therapeutic strategy for stroke. *Exp. Ther. Med.* 2018; 15: 4067-79.
14. Zhang W, Zhou X, Zhang H, Yao Q, Liu Y, Dong Z. Extracellular vesicles in diagnosis and therapy of kidney diseases. *Am. J. Physiol. Renal Physiol.* 2016; 311: F844-F51.
15. Rani S, Ritter T. The exosome - a naturally secreted nanoparticle and its application to wound healing. *Adv Mater.* 2016; 28: 5542-52.
16. Tao SC, Guo SC, Zhang CQ. Modularized extracellular vesicles: the dawn of prospective personalized and precision medicine. *Adv Sci.* 2018; 5: 1700449.
17. Chen CY, Rao SS, Ren L, Hu XK, Tan YJ, Hu Y, et al. Exosomal DMBT1 from human urine-derived stem cells facilitates diabetic wound repair by promoting angiogenesis. *Theranostics.* 2018; 8: 1607-23.
18. Biller SJ, Schubotz F, Roggensack SE, Thompson AW, Summons RE, Chisholm SW. Bacterial vesicles in marine ecosystems. *Science.* 2014; 343: 183-6.
19. Schwechheimer C, Kuehn MJ. Outer-membrane vesicles from gram-negative bacteria: biogenesis and functions. *Nat Rev Microbiol.* 2015; 13: 605-19.
20. Vanaja SK, Russo AJ, Behl B, Banerjee I, Yankova M, Deshmukh SD, et al. Bacterial outer membrane vesicles mediate cytosolic localization of LPS and caspase-11 activation. *Cell.* 2016; 165: 1106-1119.
21. Pardo YA, Florez C, Baker KM, Schertzer JW, Mahler GJ. Detection of outer membrane vesicles in *Synechocystis* PCC 6803. *FEMS Microbiol Lett.* 2015; 362: fmv163.
22. Brem H, Tomic-Canic M. Cellular and molecular basis of wound healing in diabetes. *J Clin Invest.* 2007; 117: 1219-22.
23. Driskell RR, Lichtenberger BM, Hoste E, Kretzschmar K, Simons BD, Charalambous M, et al. Distinct fibroblast lineages determine dermal architecture in skin development and repair. *Nature.* 2013; 504: 277-81.
24. Ying W, Riopel M, Bandyopadhyay G, Dong Y, Birmingham A, Seo JB, et al. Adipose tissue macrophage-derived exosomal miRNAs can modulate in vivo and in vitro insulin sensitivity. *Cell.* 2017; 171: 372-84.
25. Li J, Chen J, Kirsner R. Pathophysiology of acute wound healing. *Clin Dermatol.* 2007; 25: 9-18.
26. Sauder DN, Kilian PL, McLane JA, Quick TW, Jakubovic H, Davis SC, et al. Interleukin-1 enhances epidermal wound healing. *Lymphokine Res.* 1990; 9: 465-73.

27. Robertson FM, Pellegrini AE, Ross MS, Oberyzy AS, Boros LG, Bijur GN, et al. Interleukin-1alpha gene expression during wound healing. *Wound Repair Regen.* 1995; 3: 473-84.
28. Gallucci RM, Sugawara T, Yucosoy B, Berryann K, Simeonova PP, Matheson JM, et al. Interleukin-6 treatment augments cutaneous wound healing in immunosuppressed mice. *J Interferon Cytokine Res.* 2001; 21: 603-9.
29. Lin ZQ, Kondo T, Ishida Y, Takayasu T, Mukaida N. Essential involvement of IL-6 in the skin wound-healing process as evidenced by delayed wound healing in IL-6-deficient mice. *J Leukoc Biol.* 2003; 73: 713-21.
30. Okizaki S, Ito Y, Hosono K, Oba K, Ohkubo H, Kojo K, et al. Vascular endothelial growth factor receptor type 1 signaling prevents delayed wound healing in diabetes by attenuating the production of IL-1beta by recruited macrophages. *Am J Pathol.* 2016; 186: 1481-98.
31. Xu F, Zhang C, Graves DT. Abnormal cell responses and role of TNF-alpha in impaired diabetic wound healing. *Biomed Res Int.* 2013; 2013: 754802.
32. Eming SA, Martin P, Tomic-Canic M. Wound repair and regeneration: mechanisms, signaling, and translation. *Sci Transl Med.* 2014; 6: 265sr6.
33. Greaves NS, Ashcroft KJ, Baguneid M, Bayat A. Current understanding of molecular and cellular mechanisms in fibroplasia and angiogenesis during acute wound healing. *J Dermatol Sci.* 2013; 72: 206-17.
34. De Jong OG, Van Balkom BW, Schiffelers RM, Bouten CV, Verhaar MC. Extracellular vesicles: potential roles in regenerative medicine. *Front Immunol.* 2014; 5: 608.
35. Baouz S, Giron-Michel J, Azzarone B, Giuliani M, Cagnoni F, Olsson S, et al. Lung myofibroblasts as targets of salmeterol and fluticasone propionate: inhibition of alpha-SMA and NF-kappaB. *Int Immunol.* 2005; 17: 1473-81.
36. Hu Y, Rao SS, Wang ZX, Cao J, Tan YJ, Luo J, et al. Exosomes from human umbilical cord blood accelerate cutaneous wound healing through miR-21-3p-mediated promotion of angiogenesis and fibroblast function. *Theranostics.* 2018; 8: 169-84.